

Catalytic N–N Coupling of Aryl Azides To Yield Azoarenes via Trigonal Bipyramid Iron–Nitrene Intermediates

Neal P. Mankad, Peter Müller, and Jonas C. Peters*

Department of Chemistry, Massachusetts Institute of Technology, Cambridge, Massachusetts 02139

Received December 3, 2009; E-mail: jcpeters@mit.edu

Organoazides (N_3R) are desirable reagents for nitrene transfer reactions.¹ Generally, organoazides interact with transition metal catalysts to form transient $M-N_3R$ adduct species that in many cases subsequently extrude N_2 to yield metal-imido/nitrene (MNR) complexes as the key reactive intermediates for substrate activation.¹ Understanding the properties of metal–organoazide and metal–imido/nitrene complexes is fundamentally important in this context. Several iron–imido/nitrene intermediates that are unstable toward hydrogen atom abstraction and/or intramolecular ligand oxidation pathways have been proposed for various coordination geometries.² We³ and others⁴ have shown that iron–imido complexes formed from organoazides can be stabilized in pseudotetrahedral coordination environments. Subsequently, stable iron–imido complexes with distorted square planar geometries,⁵ as well as a trigonal planar bis(imido)iron complex,⁶ also have been structurally characterized.

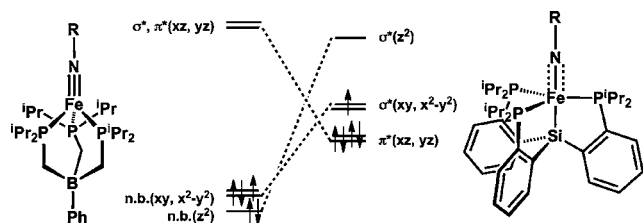


Figure 1. Qualitative d-orbital splitting diagrams for pseudotetrahedral and trigonal bipyramidal iron–imido/nitrene complexes.

An interesting geometry to consider for an $FeNR$ unit is the trigonal bipyramid (TBP). The well-studied pseudotetrahedral $L_3Fe^{III}NR$ complexes feature bona fide $Fe-N$ triple bonds resulting from two highly destabilized, unoccupied π^*_{FeN} orbitals (Figure 1, left).³ Introducing a ligand trans to the imido group and shifting the Fe into the L_3 plane in a TBP leads in principle to population of the π^*_{FeN} set (Figure 1, right), thereby obliterating a significant degree of the $Fe-N$ multiple bonding character presumed responsible for the stability of pseudotetrahedral $L_3Fe^{III}NR$ species.^{3,4a} Accordingly, until recently⁷ metal–ligand multiply bonded species in TBP configurations had been isolated only for d-electron counts of 0 or 1.⁸ TBP systems with higher d-electron counts often dissociate the apical ligand and distort toward the more stable pseudotetrahedral geometry when accommodating an axial metal–ligand multiple bond.⁹ In this context, we sought to examine the ramifications of placing a $FeNR$ linkage in a TBP environment. Our recent work¹⁰ with low-valent TBP Fe complexes supported by anionic tris(phosphino)silyl ligands ($2-R_2PC_6H_4)_3Si^-$ ($[SiP^R_3]^-$) provided a convenient entry point for such studies (Figure 1).

The addition of 1-adamantylazide to red-colored $[SiP^{iPr_3}]_3Fe(N_2)$ (**1**) produced dark brown solutions from which the organoazide adduct $[SiP^{iPr_3}]_3Fe(\eta^1-N_3Ad)$ (**2**) was crystallized. A characteristic optical band for **2** appears at 679 nm ($\epsilon = 1100 M^{-1} cm^{-1}$). The solution magnetic moment of **2** is $\mu_{eff} = 2.2 \mu_B$, consistent with an

$S = 1/2$ ground state similar to **1** and in accord with its intense electron paramagnetic resonance (EPR) signal with $g_{average} = 2.086$. The solid-state structure of **2** (Figure 2a) is noteworthy because isolable metal–organoazide complexes are unknown for Fe and are rare in general.¹¹ The η^1-N_γ binding exhibited in **2** is the most common binding mode represented in the literature.^{11a–f} The diazenylimido(2-) resonance structure ($M=N-N=NR$) is descriptive of many of these complexes^{11a–c} and results in bent $N-N-N$ angles ($114-117^\circ$) and red-shifted $\nu(N_3)$ IR bands. A recent copper(I) 1-adamantylazide complex,^{11f} on the other hand, is best formulated as a redox-innocent $RN_3 \rightarrow M$ adduct and exhibits a linear $N-N-N$ angle of $173.1(3)^\circ$ and a blue-shifted $\nu(N_3)$ IR band. Complex **2** has an $N-N-N$ angle of $147(4)^\circ$, and its N_3 vibration occurs at an energy that is indistinguishable from free 1-adamantylazide. Also noteworthy is the $Fe-N$ distance in **2** ($1.769(5) \text{ \AA}$), which is significantly shorter than that of **1** ($1.817(4) \text{ \AA}$).¹⁰ These data collectively indicate that the electronic structure of **2** lies somewhere between the above two limiting resonance structures. DFT calculations¹² are consistent with this hypothesis, as the calculated spin densities (molecular sum 1.00) on the P_3Fe and N_3 units are 1.81 and -0.77 , respectively (Figure 1c). This electronic structure is distinct from metalloradical **1**, for which 92% of the calculated spin density resides on Fe .¹²

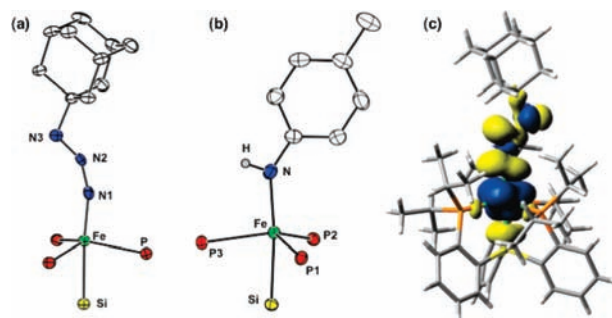


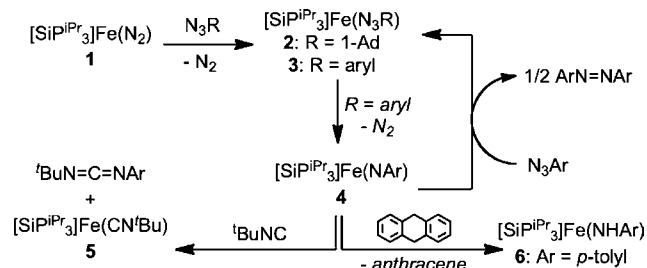
Figure 2. Core structures of (a) **2** and (b) **6** as 50% probability ellipsoids. (c) Spin density plot of **2** (0.002 isocontour). Selected bond lengths (\AA) and angles (deg) for **2**: $Fe-N1$, 1.769(5); $N1-N2$, 1.269(13); $N2-N3$, 1.25(3); $Fe-N1-N2$, 162(3); $N1-N2-N3$, 147(4); $N2-N3-C$, 111.5(15). For **6**: $Fe-N$, 1.963(2).

Stoichiometric reactions of **1** with aryl azides (N_3Ar) gave green-colored solutions that persisted at $-30^\circ C$ but that decayed gradually to yield red solutions containing **1** and the corresponding azoarene ($ArN=NAr$) products at room temperature (Scheme 1). Complex **1** also was found to be a catalyst for this unusual $N-N$ coupling reaction. With 5% catalyst loading in C_6D_6 solutions at $70^\circ C$, various aryl azides ($Ar = Ph$, p -tolyl, p - C_6H_4OMe , Mes) were converted to the corresponding azoarenes in moderate yields (44–57%). The only other spectroscopically detectable organic products were the corresponding anilines ($ArNH_2$) as minor

byproducts (8–24%).¹³ To our knowledge, the only previous example of *catalytic* N–N coupling to yield diazenes from organoazides was reported as a side reaction during the catalytic amination of C–H bonds by Co porphyrins.¹⁴ Thus, we became interested in understanding the mechanism of this unusual process.

The green intermediates observed during the reactions between **1** and aryl azides were assigned as the aryl azide complexes $[\text{Si}^{\text{Pr}}\text{Pr}_3]\text{Fe}(\text{N}_3\text{Ar})$ (**3**, Ar = Ph, *p*-tolyl, *p*-C₆H₄OMe, Mes, 2,6-Et₂C₆H₃) on the basis of in situ spectroscopic characterization and comparison to stable organoazide complex **2**. Characteristic $\nu(\text{N}_3)$ IR bands were observed at energies deviating by $\leq 3 \text{ cm}^{-1}$ from the corresponding free aryl azides, implying the presence of coordinated azide ligands. Complexes **3** are paramagnetic, and the *p*-tolyl derivative $[\text{Si}^{\text{Pr}}\text{Pr}_3]\text{Fe}(\text{N}_3\text{Tol})$ (**3-Tol**, Tol = *p*-tolyl) exhibited an intense EPR signal with $g_{\text{average}} = 2.106$. Characteristic optical bands for **3** were evident at $\lambda_{\text{max}} = 608\text{--}617 \text{ nm}$ ($\epsilon = (\text{est.}) 1400 \text{ M}^{-1} \text{ cm}^{-1}$) and ca. 775 nm (Figure 3).

Scheme 1



The decay profiles of **3** were followed by UV–vis spectroscopy at room temperature. In all cases studied, clean isosbestic behavior was observed (Figure 3), indicating that no intermediates were accumulating during the conversion of **3** to $\text{ArN}=\text{NAr}$ and **1**. The decay of **3** was found to be clean and first order (Figure 3). The rate of decay of the aryl azide complexes was relatively insensitive to the identity of the aryl substituent, as the $t_{1/2}$ of the complexes spanned a relatively small range (1.2–3.2 h at 23 °C) even as the electronics (Ar = Ph, *p*-tolyl, *p*-C₆H₄OMe) and sterics (Ar = Mes, 2,6-Et₂C₆H₃) were varied.

It is likely that complexes **3** decayed to yield reactive $[\text{Si}^{\text{Pr}}\text{Pr}_3]\text{Fe}(\text{NAr})$ intermediates (**4**) prior to N–N coupling, akin to first-order conversions of $\text{Cp}_2\text{Ta}(\text{Me})(\text{N}_3\text{Ar})$ complexes to $\text{Cp}_2\text{Ta}(\text{Me})(\text{NAr})$ studied by Bergman.^{11a,b} Important to note is our recent isolation and structural characterization of the Ru analogues of **4**, $[\text{Si}^{\text{Pr}}\text{Pr}_3]\text{Ru}(\text{NAr})$.¹⁵ Though the corresponding Fe complexes **4** are too reactive to permit isolation and thorough characterization, it appears that the *p*-tolyl derivative $[\text{Si}^{\text{Pr}}\text{Pr}_3]\text{Fe}(\text{NTol})$ (**4-Tol**) can be observed by EPR spectroscopy in a frozen glass. Photolysis of **3-Tol** in frozen 2-methyltetrahydrofuran over 1 h at 77 K resulted in a color change from green to red-brown. The disappearance of the EPR signal for **3-Tol** (Figure 4b) was accompanied by the appearance of a new EPR signal (Figure 4c) that we presume to correspond to **4-Tol**. A simulation of this signal was obtained with the parameters $(g_x, g_y, g_z) = (1.990, 2.032, 2.098)$ and $(A_x^{\text{P}}, A_y^{\text{P}}, A_z^{\text{P}}) = (55, 40, 50 \text{ MHz})$ (Figure 4d), suggesting that imido complex **4-Tol** possesses an $S = 1/2$ ground state. Upon thawing of the glass, intermediate **4-Tol** rapidly converted to **1** (Figure 4e) and $\text{ToIN}=\text{NTol}$.

Two chemical transformations further support the existence of the proposed FeNAr intermediates (Scheme 1). First, when **3-Tol** was generated in the presence of $t\text{BuNC}$, the resulting product mixture contained $\text{ToIN}=\text{NTol}$, **1**, $t\text{BuN}=\text{C}=\text{NTol}$, and $[\text{Si}^{\text{Pr}}\text{Pr}_3]\text{Fe}(\text{CN}t\text{Bu})$ (**5**). Stoichiometric¹⁶ and catalytic¹⁷ reactions

with isocyanides to yield carbodiimide products are diagnostic of isolable FeNR species. Second, when **3-Tol** was generated in the presence of 9,10-dihydroanthracene (DHA), the resulting product mixture contained a new paramagnetic product (**6**), identified crystallographically (Figure 1b) as $[\text{Si}^{\text{Pr}}\text{Pr}_3]\text{Fe}(\text{NHTol})$ after independent synthesis from $[\text{Si}^{\text{Pr}}\text{Pr}_3]\text{Fe}(\text{OTf})$ and LiNHTol . For comparison, adamantylazide adduct **2**, which does not decay at a measurable rate under analogous conditions, was found to be unreactive toward DHA and underwent ligand substitution with $t\text{BuNC}$ to yield **5** and free N_3Ad .

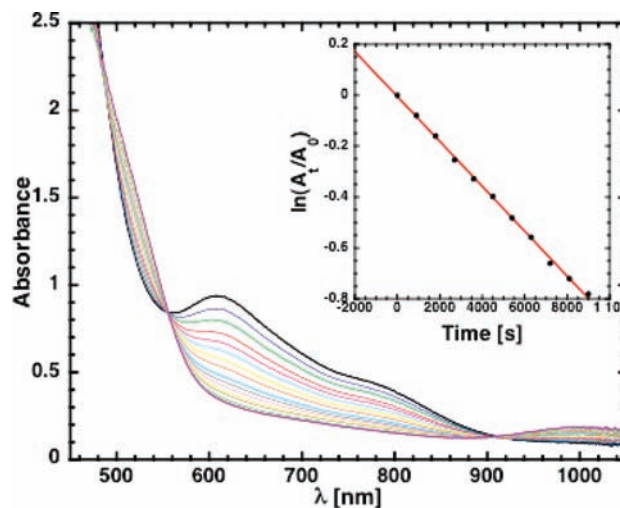


Figure 3. Changes in the UV–vis spectrum during the decay of $[\text{Si}^{\text{Pr}}\text{Pr}_3]\text{Fe}(\text{N}_3\text{Ph})$ (inset: first-order plot of absorbance at 611 nm).

Careful analysis of product distributions in these trapping experiments proved informative with regard to the mechanism of N–N bond formation. The ratio of azotoluene to anthracene decreased linearly when decreasing the concentration of **1** while holding the concentrations of N_3Tol and DHA constant (Supporting Information (SI), Table S5). If one assumes that only one Fe center is involved in the hydrogen atom transfer (HAT) reaction with DHA, this result implies the involvement of two Fe centers in the N–N bond forming step. On the other hand, the azotoluene/anthracene ratio was insensitive to varying the concentration of N_3Tol while holding the concentrations of **1** and DHA constant (see SI). Though mechanisms involving the reactions of metal-imido species with excess organoazides have been discovered for stoichiometric generation of diazenes,^{18,19} we propose for the present system that the mechanism most consistent with these product distributions is the bimolecular coupling of Fe-nitrene species **4**. Stoichiometric imido–imido coupling has been observed recently.²⁰

This finding is significant not only in the context of catalytic nitrene transfer reactions, but also because nitrene–nitrene coupling is conceptually related to oxo–oxo coupling, which may be relevant to O–O bond forming processes for some water splitting catalysts.²¹ It has been suggested that oxygen-centered radical character is crucial for such reactions to proceed.²¹ We hence chose to examine the model complex $[\text{Si}^{\text{Me}}\text{Pr}_3]\text{Fe}(\text{NPh})$ (**7**) by DFT methods¹² to explore the degree of spin character carried by the NPh moiety.

The low spin, $S = 1/2$ state (**7-LS**) was calculated to be the ground state of **7**, consistent with the EPR spectroscopy of **4-Tol** and the observed ground state of $[\text{Si}^{\text{Pr}}\text{Pr}_3]\text{Ru}[\text{N}(\text{p-C}_6\text{H}_4\text{CF}_3)]$.¹⁵ The optimized geometry of **7-LS** falls intermediate between TBP and square pyramidal ($\tau = 0.49$)²² and is similar to the crystallographically determined structure of $[\text{Si}^{\text{Pr}}\text{Pr}_3]\text{Ru}[\text{N}(\text{p-C}_6\text{H}_4\text{CF}_3)]$ ($\tau = 0.54$). The

optimized Fe–N distance in **7-LS** (1.703 Å) is much shorter than that of anilido complex **6** (1.963(2) Å). Structurally characterized Fe–NR bond distances range from 1.61–1.66 Å for tetrahedral systems^{3,4} to 1.70–1.72 Å for distorted square planar systems.⁵ Low-spin [SiP^{iPr}₃]Ru[N(*p*-C₆H₄CF₃)] has experimental and computational characteristics implying significant radical delocalization through the RuNAr π -system.¹⁵ Such delocalization is less obvious for **7-LS**, which has calculated spin densities (molecular sum 1.00) on the Fe center and NPh unit of 0.89 and 0.16, respectively, with very little spin density on the N atom itself (0.01). Noteworthy, however, are the short N–C (1.341 Å) and alternating C–C bond lengths in the calculated NPh unit of **7-LS** that suggest a significant quinoidal resonance contributor (see SI).

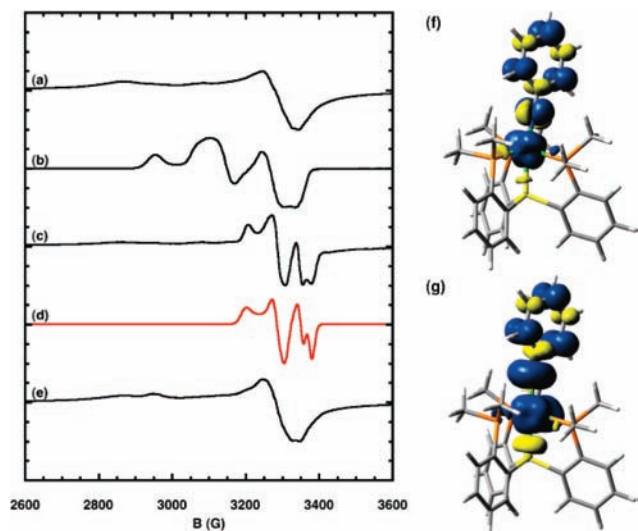


Figure 4. X-band EPR spectra (77 K, 2-methyltetrahydrofuran) of (a) **1**, (b) **3-Tol**, (c) **4-Tol** produced by photolysis of a frozen glass of **3-Tol**, (d) simulated spectrum of **4-Tol**, and (e) **1** produced upon warming and refreezing **4-Tol**; spin density plots (0.002 isocontours) of (f) **7-LS** and (g) **7-IS**.¹²

Interestingly, the intermediate spin, $S = 3/2$ state (**7-IS**) of **7** was higher in energy than **7-LS** by only 2.8 kcal/mol. The calculated spin densities for **7-IS** (molecular sum 3.00) on the Fe, N, and Ph units are 2.00, 0.82, and 0.15, respectively, indicating some radical character for the imido ligand (Figure 4).¹² Considering the likelihood that, based on our DFT studies of **7**, the [SiP^{iPr}₃]Fe(NAr) intermediates **4** also possess low-lying excited states, the possibility of two-state reactivity²³ for **4** could account for the strikingly rich redox chemistry that enables 1-electron (HAT), 2-electron (nitrene transfer), and 4-electron (bimolecular coupling) redox processes and merits further study.

Acknowledgment. This work was funded by the NIH (GM-070757). Tim Kowalczyk and Prof. Seth Brown provided helpful discussions.

Supporting Information Available: Synthetic, spectroscopic, crystallographic, and computational details. This material is available free of charge via the Internet at <http://pubs.acs.org>.

References

- (1) Cenini, S.; Gallo, E.; Caselli, A.; Ragaini, F.; Fantauzzi, S.; Piangiolino, C. *Coord. Chem. Rev.* **2006**, *250*, 1234.
- (2) (a) Eckert, N. A.; Vaddadi, S.; Stoian, S.; Flaschenriem, C. J.; Cundari, T. R.; Holland, P. L. *Angew. Chem., Int. Ed.* **2006**, *45*, 6868. (b) Lucas, R. L.; Powell, D. R.; Borovik, A. S. *J. Am. Chem. Soc.* **2005**, *127*, 11596. (c) Jensen, M. P.; Mehn, M. P.; Que, L., Jr. *Angew. Chem., Int. Ed.* **2003**, *42*, 4357. (d) King, E. R.; Betley, T. A. *Inorg. Chem.* **2009**, *48*, 2361.
- (3) (a) Brown, S. D.; Betley, T. A.; Peters, J. C. *J. Am. Chem. Soc.* **2003**, *125*, 322. (b) Brown, S. D.; Peters, J. C. *J. Am. Chem. Soc.* **2005**, *127*, 1913. (c) Thomas, C. M.; Mankad, N. P.; Peters, J. C. *J. Am. Chem. Soc.* **2006**, *128*, 4956.
- (4) (a) Nieto, I.; Ding, F.; Bontchev, R. P.; Wang, H.; Smith, J. M. *J. Am. Chem. Soc.* **2008**, *130*, 2716. (b) Verma, A. K.; Nazif, T. N.; Achim, C.; Lee, S. C. *J. Am. Chem. Soc.* **2000**, *122*, 11013.
- (5) Bart, S. C.; Lobkovsky, E.; Bill, E.; Chirik, P. J. *J. Am. Chem. Soc.* **2006**, *128*, 5302.
- (6) Ni, C.; Fetting, J. C.; Long, G. J.; Brynda, M.; Power, P. P. *Chem. Commun.* **2008**, *45*, 6045.
- (7) England, J.; Martinho, M.; Farquhar, E. R.; Frisch, J. R.; Bominaar, E. L.; Münck, E.; Que, L., Jr. *Angew. Chem., Int. Ed.* **2009**, *48*, 3622.
- (8) Betley, T. A.; Wu, Q.; Van Voorhis, T.; Nocera, D. G. *Inorg. Chem.* **2008**, *47*, 1849.
- (9) (a) Hu, X.; Meyer, K. *J. Am. Chem. Soc.* **2004**, *126*, 16322. (b) Vogel, C.; Heinemann, F. W.; Sutter, J.; Anthon, C.; Meyer, K. *Angew. Chem., Int. Ed.* **2008**, *47*, 2681.
- (10) Mankad, N. P.; Whited, M. T.; Peters, J. C. *Angew. Chem., Int. Ed.* **2007**, *46*, 5768.
- (11) (a) Proulx, G.; Bergman, R. G. *J. Am. Chem. Soc.* **1995**, *117*, 6382. (b) Proulx, G.; Bergman, R. G. *Organometallics* **1996**, *15*, 684. (c) Fickes, M. G.; Davis, W. M.; Cummins, C. C. *J. Am. Chem. Soc.* **1995**, *117*, 6384. (d) Guillemot, G.; Solari, E.; Floriani, C.; Rozzoli, C. *Organometallics* **2001**, *20*, 607. (e) Hanna, T. A.; Baranger, A. M.; Bergman, R. G. *Angew. Chem., Int. Ed. Engl.* **1996**, *35*, 653. (f) Dias, H. V. R.; Polach, S. A.; Goh, S.-K.; Archibong, D. F.; Marynick, D. S. *Inorg. Chem.* **2000**, *39*, 3894. (g) Barz, M.; Herdtweck, E.; Thiel, W. R. *Angew. Chem., Int. Ed. Engl.* **1998**, *37*, 2262. (h) Albertin, G.; Antoniutti, S.; Baldan, D.; Castro, J.; Garcia-Fontan, S. *Inorg. Chem.* **2008**, *47*, 742. (i) Waterman, R.; Hillhouse, G. L. *J. Am. Chem. Soc.* **2008**, *130*, 12628.
- (12) B3LYP, 6-31+G* for minimizations, 6-311++G** for final energy calculations. Spin densities were calculated using Mülliken population analyses (see Supporting Information for further details).
- (13) Though the complete mass balance was not accounted for in these product mixtures, we note that dark highly insoluble material was evident upon scale-up, suggesting the presence of oligomeric or polymeric material.
- (14) Ragaini, F.; Penoni, A.; Gallo, E.; Tollari, S.; Gotti, C. L.; Lapadula, M.; Mangioni, E.; Cenini, S. *Chem.—Eur. J.* **2003**, *9*, 249.
- (15) Takaoka, A.; Gerber, L. C. H.; Peters, J. C., submitted for publication.
- (16) Brown, S. D. Ph.D. Thesis. California Institute of Technology, May, 2005.
- (17) Cowley, R. E.; Eckert, N. A.; Elhaik, J.; Holland, P. L. *Chem. Commun.* **2009**, 1760.
- (18) (a) Hansert, B.; Vahrenkamp, H. *J. Organomet. Chem.* **1993**, *459*, 265. (b) Harrold, N. D.; Waterman, R.; Hillhouse, G. L.; Cundari, T. R. *J. Am. Chem. Soc.* **2009**, *131*, 12872.
- (19) See Supporting Information for data regarding crossover experiments yielding mixed diazenes.
- (20) (a) Yiu, S.-M.; Lam, W. W. Y.; Ho, C.-M.; Lau, T.-C. *J. Am. Chem. Soc.* **2001**, *129*, 803. (b) Zarkesh, R. A.; Ziller, J. W.; Heyduk, A. F. *Angew. Chem., Int. Ed.* **2008**, *47*, 4715. (c) Mansuy, D.; Battioni, P.; Mahy, J. P. *J. Am. Chem. Soc.* **1982**, *104*, 4487.
- (21) Yang, X.; Baik, M.-H. *J. Am. Chem. Soc.* **2006**, *128*, 7476.
- (22) $\tau = 0$ for an ideal square pyramid and 1 for an ideal trigonal bipyramid; Addison, A. W.; Rao, T. N.; Reedijk, J.; van Rijn, J.; Verschoor, G. C. *J. Chem. Soc., Dalton Trans.* **1984**, 1349.
- (23) (a) Klinker, E. J.; Shaik, S.; Hirao, H.; Que, L., Jr. *Angew. Chem., Int. Ed.* **2009**, *48*, 1291. (b) Hirao, H.; Kumar, D.; Que, L., Jr.; Shaik, S. *J. Am. Chem. Soc.* **2006**, *128*, 8590. (c) Dhuri, S. N.; Seo, M. S.; Lee, Y.-M.; Hirao, H.; Wang, Y.; Nam, W.; Shaik, S. *Angew. Chem., Int. Ed.* **2008**, *47*, 3356.

JA910224C